Compaction effects on evaporation and salt precipitation in drying porous media

Nurit Goldberg [1,2], Shmuel Assouline [2], Yair Mau [1], Uri Nachshon [2]

[1]The Institute of Environmental Sciences, The Robert H. Smith Faculty of Agriculture, Food and Environment, The
Hebrew University of Jerusalem, Rehovot 7610001, Israel

[2] Institute of Soil, Water and Environmental Sciences, Agricultural Research Organization,
 Rishon Lezion 7505101, Israel

Correspondence to: Uri Nachshon (urina@agri.gov.il)

Abstract

Compaction and salinization of soils reduce croplands fertility, affect natural ecosystems, and are major concerns worldwide. Soil compaction compromises soil structure and affects the soil's hydraulic properties. It therefore may have a significant impact on evaporation and solute transport processes in the soil. In this work, we investigated the combined processes of soil compaction, bare soil evaporation, and salt precipitation. X-ray computed micro tomography techniques were used to study the geometrical soil pore and grain parameters influenced by compaction. The impact of compaction on evaporation and salt precipitation was studied using column experiments. We found that compaction reduced the average grain size and increased the number of grains, due to the crushing of the grains and their translocation within the compacted soil profile. Changes in pore and grain geometry and size were heterogeneously distributed throughout the soil profile, with changes most apparent near the source of compaction, at the soil surface. The column experiments showed that the presence of small pores in the upper layer of the compacted soil profile leads to higher evaporation rates and salt precipitation, due to the compromised hydraulic connectivity to the soil surface and the prolongation of the first stage of evaporation.

1. Introduction

30 Soil compaction is a major cause of soil degradation in agricultural environments (Akker and Canarache, 2001; Hamza and Anderson, 2005; Pagliai et al., 2003). It is associated with the increase of soil bulk density and decrease of porosity (Mossadeghi-Björklund et al., 2016). Soil compaction at different intensities may occur due to natural processes such as the impact of raindrops, natural soil-forming processes, animal treading, and to processes linked to human

35 activities, especially in agricultural environments, such as intense vehicular traffic over the fields (Assouline, 2004; Pagliai et al., 2003; Shah et al., 2017; Mossadeghi-Björklund et al., 2018). Passing of heavy machinery and vehicles over the fields leads to compaction as a result of pure static stresses, wheel slip and dynamic forces, caused by vibration of the engine and the attached implements (Horn et al., 1995). Barik et al. (2014) found significant variability in

40 the spatial distribution of the aggregate stability, bulk density, total porosity, penetration resistance, and moisture content values, following traffic operation over arable lands. Pores nearby the location of compression are strongly affected, whereas those located further away from the source of compaction are less affected (Schlüter and Vogel, 2016; Keller et al., 2019). Thus, compaction resulting from traffic generally presents a sigmoidal distribution with depth

45 of the soil bulk density, where the denser part is close to the surface (Reicosky et al., 1981; Horton et al., 1994; Dejong-Hughes et al., 2001; Assouline, 2004; Bresson et al., 2004; Augeard et al., 2007).

To overcome soil compaction in arable lands and to loosen up the soil upper layer, soil tillage is implemented, producing favorable conditions for seed germination and crop root

50 development. Soil tillage reduces soil bulk density, increases porosity, homogenizes soil-wetting processes and improves soil aeration in the root zone (Rasmussen, 1999; El Titi, 2003; Assouline et al., 2014; de Almeida et al., 2018). On the other hand, under certain conditions, tillage may accelerate processes of soil erosion and compaction of the soil at the lower

boundary of the tilled zone (de Almeida et al., 2018). Therefore – minimizing tillage and better

55   understanding of the nature of soil compaction is important.

1.1. Soil compaction at the micro-scale

At the microscale, stresses in soil do not propagate homogeneously but rather through

preferential paths – in all directions (Nawaz et al., 2013). Consequently, soil deformation

occurs at specific sites, where the stresses and strains are maximal. These areas, known also

60   as shear bands, are those that undergo structural deformation, while soil volumes in between

the stress chains may preserve their original structure and porosity (Nawaz et al., 2013;

Naveed et al., 2016). The heterogeneous effect of compaction on the physical properties of

the soil leads to an uneven spatial distribution of the soil's hydraulic properties that in turn

induce anisotropy and affect water flow and solute transport processes in the soil profile

65   (Assouline, 2006a; b; Assouline and Or, 2006; Alaoui et al., 2018).

Soil compaction affects the pore network in the soil profile, with respect to: (i) pore-size

distribution; (ii) pore geometry and morphology; and (iii) pore connectivity (Horn et al., 1995;

Mossadeghi-Björklund et al., 2016). Consequently, water-related soil properties are

significantly altered (Horn et al., 1995; Assouline, 2006a; b). These changes affect unsaturated

70   soil hydraulic properties and reduce saturated soil hydraulic conductivity, thus increasing

surface runoff and soil erosion by water (Soane and van Ouwerkerk, 1995; Alaoui et al., 2011;

Keller et al., 2013; Shah et al., 2017). In addition, soil aeration is reduced and the

heterogeneous changes of the soil's physical and hydrological properties, may lead to the

formation of preferential water flow paths in the soil (Soane and van Ouwerkerk, 1995; Alaoui

75   et al., 2011; Keller et al., 2013). Consequently, solute transport and accumulation in the soil

may be affected, impacting nutrient availability to plants (Horn et al., 1995; Lipiec and

Stępniewski , 1995; Hendrickx and Flury, 2001; Mossadeghi-Björklund et al., 2016). The

above-mentioned changes of the soil properties, due to compaction, usually occur at the top

30 cm of the soil profile (Horn et al., 1995; Keller et al., 2019). These changes in the soil

80 structure of the upper soil layer impacts on the soil water balance in general, and on

infiltration and evaporation processes in particular (Sillon et al., 2003; Assouline et al., 2007,

2014; Shokri et al., 2010).

1.2. Bare soil evaporation

Evaporation plays a central role in the hydrologic cycle and surface energy balance (Bergstad

85 et al., 2018) as it is the main process of soil-water transfer to the atmosphere (Hillel, 1980;

Brutsaert, 2005). The evaporation in porous media is affected by and involves complex and

highly dynamic interactions between boundary conditions, liquid flow and vapor diffusion

(Lehmann et al., 2008; Or et al., 2013; Assouline et al., 2014; Kamai and Assouline, 2018;

Assouline and Kamai, 2019). The evaporation process from bare soils consists of two stages:

90 stage 1 (S1); and stage 2 (S2). S1 evaporation takes place at the soil surface, and a hydraulic

connection is maintained throughout the entire soil profile (Lehmann et al., 2008; Nachshon

et al., 2011a; b; Bergstad et al., 2018; Assouline and Narkis, 2019). This stage is characterized

by a high and relatively constant evaporation rate affected by soil surface properties and

atmospheric conditions (Hillel, 1980). S2 begins when a characteristic capillary head, ψ_c, is

95 reached at the soil surface that induces a loss of the hydraulic connection between the soil

profile and the surface (Prat, 2002; Lehmann et al., 2008). Consequently, the evaporation

front migrates downward, water vapor moves prominently by diffusion from the evaporation

front to the soil surface and to the atmosphere, and the evaporation rate is drastically reduced

(Lehmann et al., 2008; Nachshon et al., 2011b; Or et al., 2013; Kamai and Assouline, 2018).

100 ### 1.3. Evaporation and soil salinization

Evaporation and soil salinization are tightly connected processes, especially in cultivated

fields. Soil salinization in cultivated fields is a common feature resulting from low-quality

irrigation water, fertilization, and saline and shallow groundwater resulting from inadequate

irrigation and drainage practices (Yakirevich et al., 2013; Berezniak et al., 2018; Nachshon, 2018; Hopmans et al., 2021).

The presence of salts in the soil pore water reduces the osmotic potential of the solution and the equilibrium water vapor pressure (Nassar and Horton, 1997). Consequently, evaporation rates from a saline soil are expected to be lower compared to solute-free conditions. During evaporation, the concentration of the dissolved ions increases in the pore solution, until saturation is reached and salt precipitation begins (Nachshon et al., 2011a). Salt precipitation at the soil surface occurs manly during S1, where the evaporation rate is maximal and solutes are continuously transported to the evaporation front at the soil surface by capillary flow. As the salt begins to precipitate and expands over the soil surface, the evaporation rate is affected by the pore-scale dynamics of the precipitated salt (Bergstad et al., 2017, 2018), and the consequent changes to liquid and vapor flow processes through the salt crust. The presence of porous media heterogeneities (Lehmann and Or, 2009; Nachshon et al., 2011b), solute concentration of the pore water (Rad and Shokri, 2012; Shokri-Kuehni et al., 2017), soil surface properties (Nachshon et al., 2011a) and salt type (Shokri-Kuehni et al., 2017) may affect the dynamics of the salt precipitation layer and its influence on evaporation (Bergstad et al., 2018). The precipitated salt layer over the soil surface may increase evaporation if it is hydraulically connected to the solution in the pores below. In this case, the precipitated salt, that usually has a higher surface area compared to the underlying bare soil, pumps water upward due to its higher capillary suction, and the water evaporates at the surface of the precipitated salt crust (Shokri-Kuehni et al., 2017). On the other hand, if the precipitated salt layer is hydraulically disconnected from the solution in the pores, it acts as a barrier that reduces vapor diffusion from the soil to the atmosphere, and cumulative evaporation and evaporation rates will be reduced (Nachshon et al., 2011b).

Previous studies have shown that changes in soil structure affect evaporation processes (Nassar and Horton, 1999; Sillon et al., 2003; Shokri et al., 2010; Assouline et al., 2014;

130 Assouline and Narkis, 2019) as well as the nature and location of salt precipitation in the presence of saline solution (Nachshon et al., 2011b; a; Bergstad et al., 2017). The drying patterns and dynamics are greatly influenced by the presence of textural discontinuities that may result in preferential drying and promotion of capillary exchange between different regions in the soil (Lehmann and Or, 2009; Bergstad et al., 2017). As aforementioned, soil

135 compaction affects soil structural and textural properties, mainly at the soil surface, where evaporation and salt precipitation are prominent.

1.4. Evaporation and soil compaction

Studies on the effect of soil compaction on evaporation, in general, and its relation to salt precipitation in particular, are scarce. Nassar and Horton (1999) examined salinity and

140 compaction effects on soil water evaporation from bare soils, focusing on water and solute distributions in the soil. They showed that compaction increases cumulative evaporation, due to increased matric suction of the compacted soil, resulting in the increase of the soil water holding capacity and unsaturated hydraulic conductivity. Consequently, water flows more efficiently from deep parts of the soil profile to the soil surface, where evaporation is maximal,

145 at S1 evaporation. In their study, Nassar and Horton (1999) deliberately compacted the soil samples in a homogeneous manner, ignoring the heterogeneous nature of soil compaction. Moreover, while the authors examined the impact of compaction and evaporation on solute distribution in the soil profile, and its impact on the solution osmotic potential, they did not consider the interactions between soil compaction, evaporation, and salt precipitation.

150 Sillon et al. (2003), using indirect measurements under non-saline field conditions, also pointed at higher evaporation from compacted soils. The authors showed that for compacted soils, soil drying occurred from bottom to top, in opposition to regular evaporative conditions,

where the drying (evaporation) front recedes from the surface downward. In agreement with Nassar and Horton (1999), this was explained by the high capillary suction of the compacted

155   soil that enabled pumping of water from the lower parts of the soil profile to the soil surface, where evaporation takes place. Assouline and Narkis (2019) used a constructed multilayered porous media, where the top layer had the highest bulk density, smallest grains, and smallest pores, and where the bulk density gradually decreased, while grains and pore sizes gradually increased in the underlying layers. They have measured evaporation from this structure and

160   from a structure where the order of the layers was reversed. It was shown that the soil structure where the top layer had the highest bulk density extended the S1 duration and increased the cumulative evaporation in comparison to the reversed structure. The concept of the characteristic length was applied to explain these results, providing a physically-based support to the observations of Sillon et al. (2003).

165   The main objective of the work presented herein is to understand the impact of soil compaction on soil evaporation, solute distribution and salt precipitation, and their interactions, along the soil profile. Relying on previous works (Nassar and Horton, 1999; Sillon et al., 2003; Assouline and Narkis, 2019), we conducted a series of experiments to fill up the knowledge gaps regarding the complex interactions between the heterogeneous structural

170   nature of compacted soils, evaporation, and salt dynamics.

2. Conceptual model

Based on the studies detailed above, we hypothesize that compaction results in a layered structure where soil bulk density is maximal at the soil surface and gradually decreases

175   downward (**Figure 1A**). Consequently, capillary suction, water holding capacity and unsaturated hydraulic conductivity of the upper layer of the soil profile increase, as well as its characteristic capillary length, thus increasing the duration of S1 (Lehmann et al., 2008). Under

non-compacted conditions, the evaporation front of a drying porous medium moves from the soil surface downward at the transition from S1 to S2 (**Figure 1B(1)**). However, in a compacted

180 soil profile, the larger matric potential (ψ_c) value of the upper soil layer leads to a reverse process, where a continuous flow of water is sustained from the deeper layer of the soil profile to the soil surface, extending the duration of S1 and allowing more water to evaporate. Consequently, the deeper soil layers dry out first, while the upper layers remain at relatively high levels of water content (**Figure 1B(2)**).

185 Under saline conditions, where the pores are filled with a salty solution, evaporation will lead to solute precipitation at the soil surface, and to the formation of an efflorescence salt crust, at least in the case of NaCl (Nachshon and Weisbrod, 2015; Piotrowski et al., 2020). In non-compacted conditions, the precipitated salt crust reduces evaporation as it acts as a barrier that reduces water vapor diffusivity from the evaporation front to the soil surface and to the

190 atmosphere (**Figure 1B(1)**). On the other hand, in the compacted soil condition, it is hypothesized that a hydraulic connection will be maintained between the soil profile and the surface of the salt crust (**Figure 1B(2)**), where evaporation will take place. Therefore, we hypothesize that even though more salt is expected to accumulate on the surface of the compacted soil, its impact on evaporation will be moderate compared to non-compacted
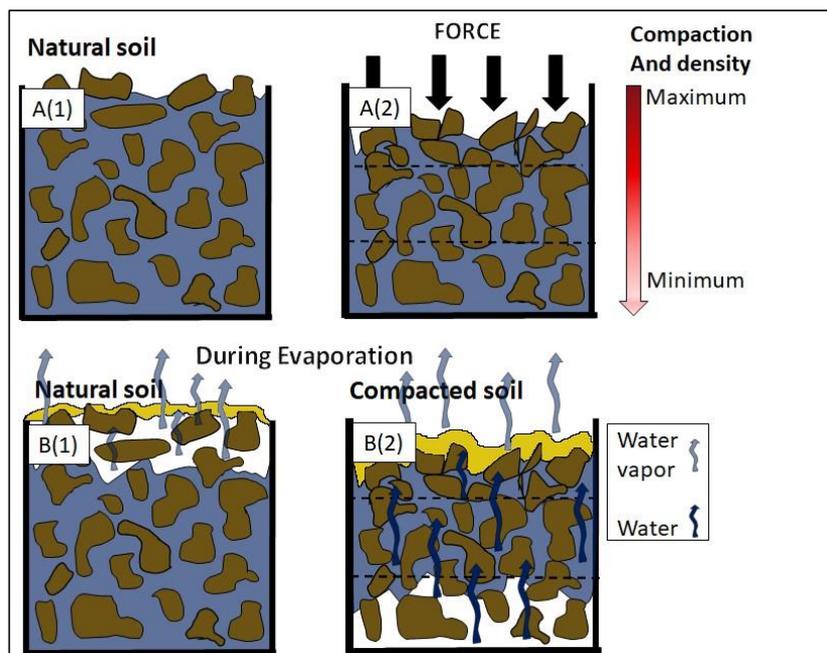
195 conditions.

200

Figure 1: Conceptual model of evaporation and salt precipitation under compacted and non-compacted conditions; (A) initial saturated conditions for neutral (non-compacted) and compacted soils; (B) Water evaporation process in neutral and compacted soils, with the presence of a precipitated salt crust (yellow layer).

205

These hypotheses were tested herein by means of high-resolution micro CT to characterize, at the micro scale, the impact of compaction on soil pores and grains properties, and column experiments to study the impact of compaction, at the macro-scale, on evaporation and salt precipitation.

210

3. Materials and method

This study relies on three parts: (i) exploration of the impact of compaction on soil physical properties at the micro and macro scales; (ii) numerical simulation of evaporation from a layered domain, mimicking compacted and loose porous media, with and without the

215   presence of a precipitated salt crust; and (iii) validation of the conceptual model presented in

Figure 1 by means of evaporation experiments.

3.1. Micro scale changes of pores and grains physical properties due to compaction

Imaging of sand samples before and after compaction was conducted in a non-destructive

manner using a high-resolution µCT (SKYSCAN 1172, Bruker, Kontich, Belgium), in order to

220   observe the impact of compaction on the sand physical structure, pores and grains

dimensions, and spatial arrangement. The X-ray source voltage was 80 kV, and the electrical

current, 10 mAs. The scan was done with aluminum and copper filters, with image rotation of

0.2°. Images with voxel resolution of 4.42 µm were reconstructed by the software 'NRecon'

(Bruker, Kontich, Belgium). Image analyses were carried out using designated MATLAB codes.

225   Polyvinyl chloride (PVC) tubes, 3-cm-long and 1.6-cm in diameter, open at the top and sealed

at the bottom, were filled with quarry coarse sand (quartz), with typical grain diameter of

~500 µm (sand characteristics can be found in Nachshon, 2016). The columns were scanned

before and following mechanical compaction, in order to detect the impact of compaction on

microscale changes of the sand properties, as a function of depth and distance from the source

230   of compression. Compaction was achieved using a PVC shaft that fits exactly the inner

diameter of the column. The shaft was slowly pushed downward to compress the sand

samples, using a hand-operated press, achieving a one-dimensional confined compression.

The samples were compressed down to a decrease of the total length of the sand sample by

2 mm, corresponding to an increase of 10% of the packing bulk density of the samples.

235   The images from the µCT scans were used to analyze grain and pore sizes at the top 7 mm of

the sand samples and at depth of 9-18 mm. Hereafter, the top and lower levels of the

compacted samples will be referred to as 'TC' and 'LC', respectively, and the non-compacted

control will be referred to as 'UN'. The TC and LC results were used to compare the impact of

compaction at the top and the lower layers of the sample. Each µCT scan generates hundreds

240   of images of 2D slices of the sample, with a 4.42 µm distance between adjacent slices. For

each scan, five 2D images, out of the hundreds of images, were chosen randomly, processed,

and analyzed by a MATLAB code. Grayscale calculations were based on Otsu's method, which

selects the threshold to minimize the interclass variance (Otsu, 1979). Morphological

operations were done to clean image noises. Grain counting and grain area calculations were

245   done using the MATLAB function '*regionprops*'. A distance heat map was generated using the

Euclidean distance transform, '*bwdist*' and the MATLAB function '*bwskel*'. Pore sizes were

obtained by calculating the average maximal pore distance from the closest grain edge along

the pores and throats. Grain distribution map was generated by counting the center of each

grain.

250   **3.2. Macro scale changes at the soil profile due to compaction**

While the µCT experiments described above were used to study the effect of compaction at

the pore scale, a transparent 10 cm long and 5 cm in diameter PVC column was used to

examine the effect of compaction at the macro scale. The same coarse sand as detailed above

was used in this experiment. To allow visual observation of changes in the compacted sand

255   column, 10% of the sand (by weight) was colored with a standard red spray paint. The colored

sand was thoroughly mixed with the regular sand, before packing the column.

As described previously, the sand in the column was compacted by decreasing the total length

of the sand sample by 5 mm, using a uniform hammer beating on a circular shaft, with the

same diameter as the inner diameter of the PVC column. The bulk density of the sand sample

260   was reduced by ~5% following compaction.

Pictures of the sand column profile were taken before and after compaction by a single lens

reflex camera (Canon - EOS60D, Japan), with an EFS18-200 mm lens (Japan). Compaction was

evaluated by analyzing the images that captured the movement of the colored sand grains

and measuring the translocation of the same colored grains before and after compaction.

3.3. Numerical model

A preliminary analysis, to estimate the general impact of soil compaction on evaporation, with and without the presence of a precipitated salt crust, was carried out based on simulations using HYDRUS-1D (Šimůnek et al., 2013), for a compacted domain and a neutral (non-compacted) domain. Under the assumption that compacted soil is most affected at the soil surface, where compression forces are maximal, the simulated compacted domain was composed of five discrete layers, 2 cm each, where the most upper layer had the highest bulk density, smallest grain diameter, lowest saturated hydraulic conductivity and highest air entry pressure. Underlying layers were gradually comprised of bigger particles, lower bulk density, higher hydraulic conductivity and lower air entry pressure, as detailed in **Table 1**. For the neutral domain, the same particles that were selected to compose the discrete layers of the compacted domain were homogeneously mixed and its hydraulic properties are detailed in **Table 1** also.

The sizes of the particles at the different modeled layers were determined upon real physical sizes of glass beads that were used in the column experiments that will be presented in the next section. Saturation water content, θ_s, was determined experimentally by measuring the volume of water needed to saturate the different glass beads that were packed in a known volume. Residual water content, θ_r, was taken as zero, since full drying of glass beads can be reached by evaporation. The van Genuchten parameter α was determined according to Benson et al. (2014) that correlated α to particles diameter. The van-Genuchten n parameter is affected by the degree of grain uniformity in the domain (Wang et al., 2017), where high n values indicate on high uniformity. Therefore, n was taken as 3 for the uniform layers, as it was the highest n value permitted by HYDRUS, and for the homogeneously mixed domain, n was arbitrarily chosen to be equal to 1.25 as the medium was composed of particles with various sizes. Hydraulic conductivity at saturation, K_s [cm/d], was determined by the Kozeny-Carman equation (Kozeny, 1927; Carman, 1937), as demonstrated by Weisbrod et al. (2013)

Table 1: Hydraulic parameters for the HYDRUS-1D modeled glass beads.

Modeled domain	Depth (mm)	Particles diameter (mm)	Residual water content	Saturation water content	Van-Genuchten parameters		Hydraulic conductivity K_s (cm/d)
			Q_r (-)	Q_s (-)	α (1/cm)	n (-)	
Compacted	0-20	0.049 – 0.053	0	0.395333	0.010133	3	232.5494
	20-40	0.090 – 0.106	0	0.36	0.015199	3	578.7839
	40-60	0.180 – 0.212	0	0.380667	0.035464	3	2922.904
	60-80	0.400 – 0.500	0	0.296667	0.070928	3	5654.909
	80-100	1.000 – 1.300	0	0.415	0.151988	3	146131.9
Non-compacted	0-100	Homogeneous mixing of all beads	0	0.283333	0.050663	1.25	3537.92

295

The modeled domains had a depth of 10 cm and the upper boundary condition was set as

atmospheric boundary, with potential evaporation of 0.65 cm/d (based on the data obtained

in the laboratory glass-beads evaporation experiment, which will be detailed below). Lower

boundary was set as zero flux and initial condition was set as full saturation throughout the

300 entire column. Since HYDRUS solves the Richards equation, its results are valid only during

S1 where evaporation is occurring at the soil surface and there is a hydraulic continuity along

the soil profile. Therefore, simulations were ceased once S1 was ended and the transition to

S2 begun.

The simulations were used to observe changes of the soil profile wetness and to compute

305 cumulative evaporation for the compacted and neutral setups, with and without the

presence of a salt crust. The salt crust was simulated by adding a 2 mm layer on top of the

modeled domains (this thickness is similar to the observed one corresponding to the

depositing salt layers during the experiments presented below). This layer was added after

two days of evaporation, as it is experimentally known that the appearance of the salt crust

310 is not instantaneous with the onset of evaporation. The hydraulic properties of a salt layer

are unknown, excluding permeability, k, which was recently examined, and found to be at

the order of 4×10^{-12} m^2, for NaCl (Nachshon and Weisbrod, 2015; Piotrowski et al., 2020).

The permeability was used to calculate the saturated hydraulic conductivity of the salt, by

the relation between K_s and k (Kasenow, 2002):

315 $$K_s = \frac{k \cdot \rho \cdot g}{\mu} \qquad\qquad\qquad (1)$$

where μ [kg/ms] is the dynamic viscosity; ρ [kg/m^3] is the liquid density; and g [m/s^2] is gravity

acceleration. For water, ρ = 1000 [kg/m^3], and $\mu \sim$ 0.0009 [kg/ms] (at 25°c). g = 9.8 [m/s^2],

and for the NaCl permeability of 4×10^{-12} [m^2] K_s is equal to 4.35556 × 10^{-5} [m/s] = 376.32

[cm/d]. Since no further information is available about the salt hydraulic properties, the van-

320 Genuchten parameters of the salt layer were taken to be equal to loamy-sand soil, from the

HYDRUS-1D library, due to the similar hydraulic conductivity that this soil (350.2 cm/d) has

to the salt layer. Important to emphasize is that the model examined only the physical impact

that a salt crust has on water flow process during S1 and did not account for the chemical

aspects of high salinity and the reduction of the solution osmotic potential.

325 **3.4. Impact of compaction on evaporation and salt precipitation**

The evaporation experiments were conducted on rectangular glass columns, 10 cm high, 5 cm

width, and 2.5 cm aperture. The neutral and compacted columns were packed with glass

beads of different sizes and different arrangements, as detailed in **Table 1**. In this set of

experiments, a setup of tilled soil was examined also and for this purpose the tilled setup was

330   constructed in a reverse order of the compacted setup, with the largest glass beads at the top

of the profile and the smallest beads at the bottom.

The three different setups were saturated with distilled water (DI) or with a 10% (by weight)

NaCl solution. All the evaporation experiments were carried out in two replicates. The

packed columns were positioned on high resolution electronic scales (±0.01 gr, Adam;

335   Shekel, Israel) in order to record mass changes, thus monitoring the cumulative water loss

to evaporation. Small fans (Y.S. TECH, DC BRUSHLESS FAN, FD128020HB, DC12V, 0.15V) were

installed ~3 cm above the upper soil surfaces of the samples, pulling air upward. Along the

process of evaporation, photos of the columns profiles were taken with a camera (UEye,

Germany) at a rate of 6 pictures per minute. Total duration of evaporation for each setup

340   was about 12.5 days (~303 hours).

4.   Results and Discussion

Experimental results are organized and presented first, for the micro-scale, and then for the

macro scale; considering the physical changes that the sand underwent due to compaction.

345   Following that, the results representing the impact of compaction on the combined processes

of evaporation and salt precipitation will be discussed.

4.1. Micro-scale effects of compaction

The impact of compaction on changes in grain and pore geometry, size and distribution, at the

micro scale, were examined by producing 2D images (slices) of the sand domain using the μCT.

350   **Figure 2** presents a qualitative description of the changes in pore and sand grain properties

following compaction at the top layer of the sample and at its bottom. **Figure 2a** presents

representative images from: (i) an uncompacted sample (UN) at depth of 0-7 mm (**Figure 2a'**);

(ii) the lower part of the compacted sample (LC; depth of 9-18 mm) (**Figure 2a''**); and (iii) the

top part of the compacted sample (TC; depth of 0-7 mm) (**Figure 2a'''**). In the UN, as well as in

355 the LC domain, the sand grains are relatively round and uniform in size. By comparison, in TC,

there are areas with high proportion of relatively small and more angular grains, a result of

the grains breakage in specific locations (marked by the yellow contours in **Figure 2a'''**).

Naturally, these changes in grain sizes also affect pore sizes and their spatial distribution, as

depicted by the pores opening heat map (**Figure 2b**).

360 In **Figure 2c,** we represent the changes in grain sizes in the TC sample and the spatial

distribution of these changes, in comparison to the UN and LC data. For this purpose, each 2D

scan, of any state and depth, was divided into a matrix of rectangles, 1.06 mm by 0.73 mm,

each. In each rectangle, the number of sand grains was counted, and the rectangle was

colored in accordance to the number of grains. In the presented images, the main colors for

365 the LC and UN cases are blue and green, indicating about 3-4 grains per rectangle, with low

variation in colors. However, for the TC case, there is a high variation in the color of the

rectangles, with a relatively high number of yellow and red rectangles (>6 grains) adjacent to

green-blue rectangles.

The five randomly selected images of 'UN', 'TC', and 'LC' states were averaged and analyzed

370 to provide a corresponding quantitative analysis of the number of grains per unit area, grain

size (2D area) and pore opening (distance between adjacent grains) (**Figure 3**). For simplicity,

all of these values were normalized with respect to those corresponding to the UN state. In

agreement with the visual observations, minor differences were measured with respect to the

number of grains between the UN and LC states. However, a significant difference was

375 measured with the TC samples, where the total number of grains, per unit area, was ~50%

higher for TC compared to UN and LC (**Figure 3A**). Moreover, with respect to changes in grain

sizes, there is no significant difference between UN and LC, but for the TC layer, the average

size of the grains was ~35% lower compared to UN and LC cases. The same trend was

measured also with respect to pore opening, as the pore average opening of the TC was lower

380 by ~10% compared to the two other cases.
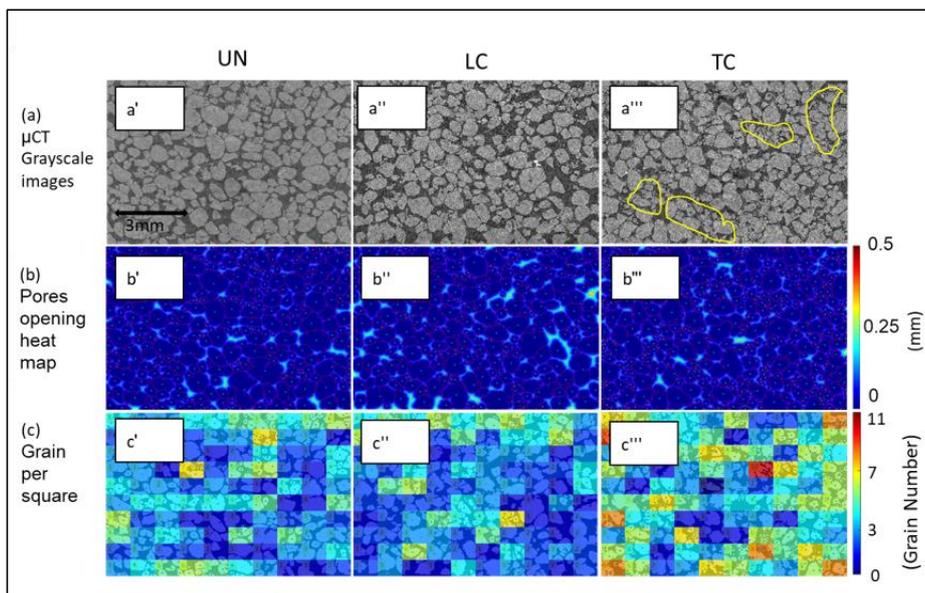
Figure 2: (a) µCT grayscale scan; (b) pore opening heat map; and (c) grain number spatial distribution map, for the uncompacted ('), low (") and top ("') levels of compacted soil samples, respectively. Yellow contours in (a"') indicate areas with high levels of grains breakage. In (b), the blue dots represent the grain centers and the color bar indicates the distance within the pores from the nearest grain. In (c), the rectangles are colored in proportion to the number of grains in each one of them.

The analysis of the grain counting within the rectangles (**Figure 2c**) was also conducted for the

390 five randomly selected images. Analysis of each image was used to generate a histogram

describing how many rectangles contained the different numbers of grains (**Figure 3B**). For

the UN and LC cases grain density was lower compared to the TC setup, where the former had

on average 2-2.5 grains per rectangle, whereas the latter had 4 grains per rectangle.

Moreover, for the TC layers, in comparison with the LC and UN cases, the histogram shifts to

395 the right, indicating a higher number of rectangles that contain 4 grains or more.
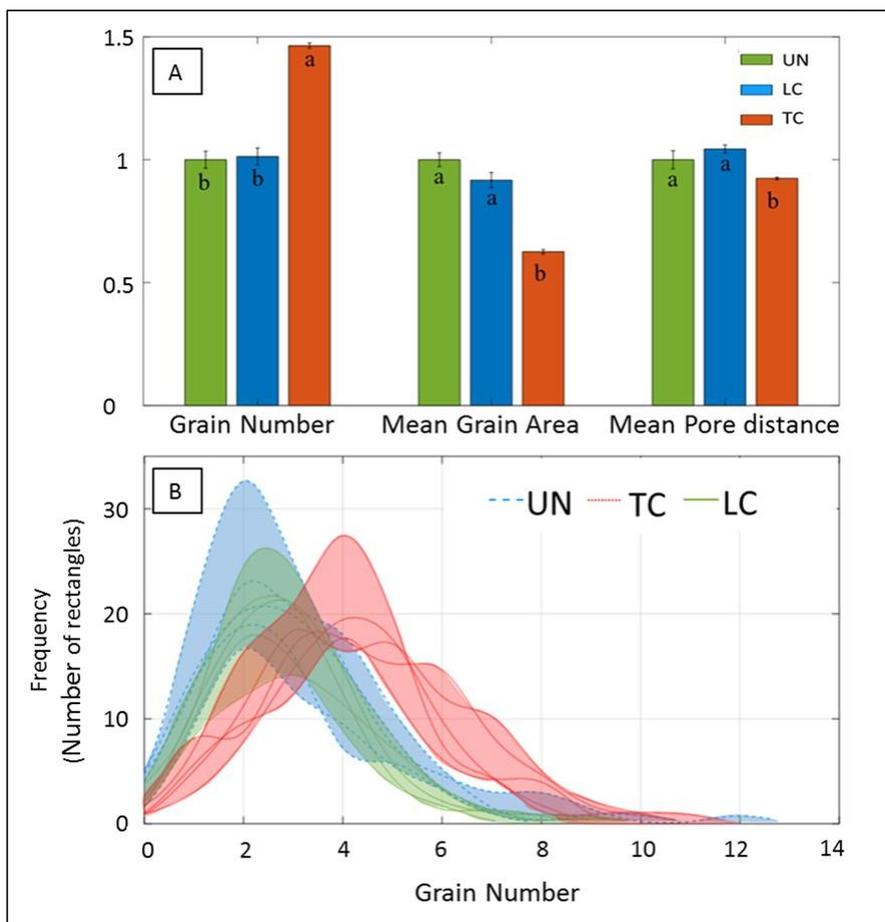
Figure 3: (A) Average grain number, average grain area and average pore distance of the uncompacted soil sample (UN), low (LC) and top (TC) levels of compacted soil samples. Measured values were normalized in respect to UN. (B) Histogram represents grain number distribution of the uncompacted soil samples, and low and top levels of the compacted soil samples. In (B), each line is the histogram of a single slice and the colored areas represent the range of the five measured histograms, for each state.

The presented image analyses, at the micro-scale, indicate the major impact that compaction

has on the physical properties of the sand, close to the source of compaction (TC). It seems

that compaction resulted in breakage due to friction of sand grains, leading to an increase in

the grain number and their angularity, and a decrease in their mean size. In the deeper layer

of the sand column (LC), the grains were practically not affected by the compaction and were

similar to the control (UN) with respect to pore and grain sizes, shape and spatial distribution.

410   Moreover, it was shown that the compacted areas in the top layer were heterogeneously

distributed (**Figure 2c, 3B**), in agreement with the concept of preferential propagation of the

stress along the 'shear bands' (Nawaz et al., 2013; Naveed et al., 2016).

4.2. Macro-scale effects of compaction

At the macro scale, compaction effects were quantified by following the translocations of the

415   colored sand grains, in the 10-cm-long transparent column. The translocation of the sand

grains, ΔL [mm], was calculated by measuring the distance of selected grains from the

column's bottom at the initial state (L_0) and following compression (L_C), according to:

$$\Delta L = L_C - L_0. \tag{2}$$

Figure 4 presents ΔL along the soil profile. Maximal translocation was observed within the

420   upper layer of the soil profile, and it linearly decreases with depth, in agreement with the

results reported by Schlüter and Vogel (2016). However, it is important to remember that

translocation of the grains at each depth is the sum of all compaction processes that occurred

below the point of interest, and that it does not necessarily indicated the degree of

compaction (change of bulk density) at this point. In order to estimate the effect of

425   compaction on the bulk density along the soil profile we estimated the changes in distance

between adjacent grains, ΔD [mm], in a similar way that it was done for ΔL:

$$\Delta D = D_C - D_0 \tag{3}$$

where D_0 and D_C are the measured distances between any adjacent selected grains, before

and following compaction, respectively. Consequently, a negative ΔD value indicates

430   compaction and increase in bulk density, and vice versa.

Measurements of ΔD indicate that compaction was not uniform along the sand profile (**Figure**

4), showing that certain depths were more severely compacted. At depths of 6, 17, 36, and 60

mm, ΔD values were positive, indicating reduced bulk density at these specific locations.

Maximal compaction of ΔD = -1.3 mm was measured at a depth of 32 mm, followed by ΔD =

-1.1 mm at depth of 8 mm. Lower levels of the column were less compacted, excluding depths

of 68 and 82 mm where ΔD reached values of -1.0 and -0.8 mm, respectively.

This analysis further emphasizes the heterogeneous nature of soil compaction and the shear

band effect. Nevertheless, it is evident that most of the profile underwent compaction, as

most of the ΔD values are negative, and that maximal compaction was measured in the top

parts of the sample, in agreement with the results from the micro-scale study.
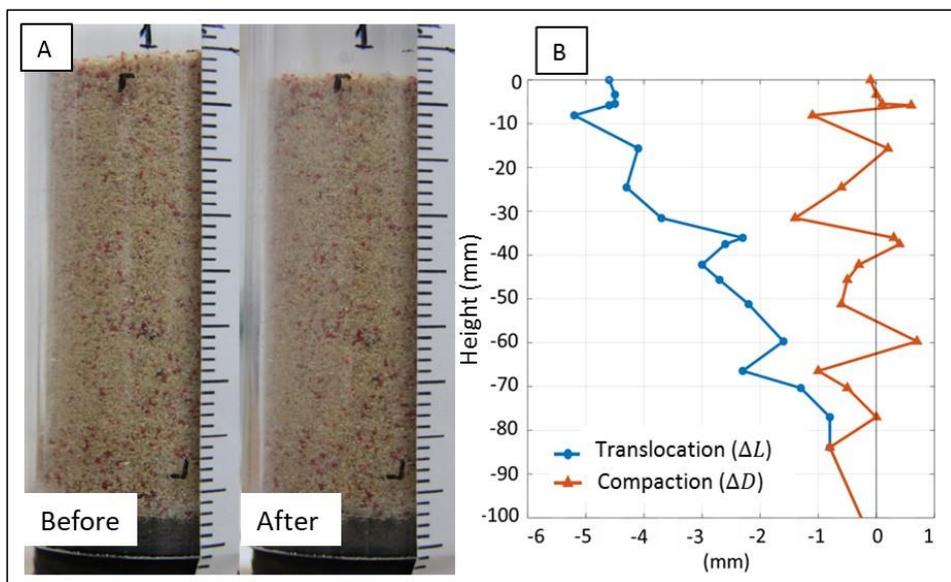
Figure 4: (A) photos of the examined sand column 'Before' and 'After' compaction; **(B)** measured changes in grains translocation and compaction along the sand column.

As seen from the micro and macro scales experiments, compaction induces the formation of

a non-uniform soil profile, with smaller pores, smaller grains, and higher bulk density at the

top levels of the soil profile, compared to the lower part of the profile. This structure is

opposed to typical natural conditions, where the lower soil levels are those with the higher

bulk density (Campbell, 1994; Hernanz et al., 2000). Consequently, important hydrological

450   processes such as infiltration and evaporation may be altered due to compaction. These

aspects will be discussed in the following sections.

4.3. Numerical model

The HYDRUS-1D model results showed similar trends to those proposed in the conceptual

model and in the research hypothesis, including the unique pattern of drying from top to

455   bottom, for the layered structure with the fine grains at the top. **Figure 5** presents temporal

changes in water content along the modeled domain and cumulative evaporation predicted

by the model, for neutral - homogeneous setup (HO), and compacted setup with the finer

pores and grains at the upper parts of the simulated domain (FU). The simulations were done

for conditions of with and without the salt crust. As detailed above the simulations were

460   ceased at the transition from S1 to S2.

From **Figure 5** it is seen that for salt free conditions, the FU setup sustained a longer S1

duration (~130 hours), compared to the HO setup (~72 hours). Consequently, cumulative

evaporation during S1 of the FU setup was more than 40% higher, compared to the HO setup

which shows a cumulative evaporation of ~2cm. The temporal changes in water content gives

465   the physical explanation for that, showing that the FU structure maintains higher water

content levels at the upper soil layers due to the stronger capillary suction of these layers,

which pump water from the lower levels, towards the evaporation front, at the soil surface.

Moreover, it is seen that while the addition of the modeled salt layer had a major impact on

evaporation for the HO setup, its effect on the FU structure was more moderate. For the HO

470   structure, the addition of the salt layer resulted in an immediate transition to S2, with a sharp

decrease in evaporation rate and reduced cumulative evaporation at the end of S1 by ~35%,

compared to the HO salt free setup (**Figure 5 A1**). The quick transition to S2 indicates that for

the HO conditions, after two days of evaporation and the resulted changes of water saturation

along the profile, the presence of the salt crust resulted in hydraulic discontinuity between

475   the saturated lower parts and the upper surface of the domain. For the FU structure, however,

less noticeable changes in evaporation rates were observed following the addition of the salt

layer, S1 sustained for additional ~48 hours, with the presence of the salt layer and the

reduction in cumulative evaporation was of ~12% only. This indicates that the added salt layer

did not affect liquid water flow from the soil to the evaporation front, which is now located

480   on top of the added salt layer (**Figure 5 B1**). The fine media at the top of the FU profile

maintained wetness conditions that enabled liquid water flow from the soil into and through

the salt layer, to replenish evaporation at its upper surface.
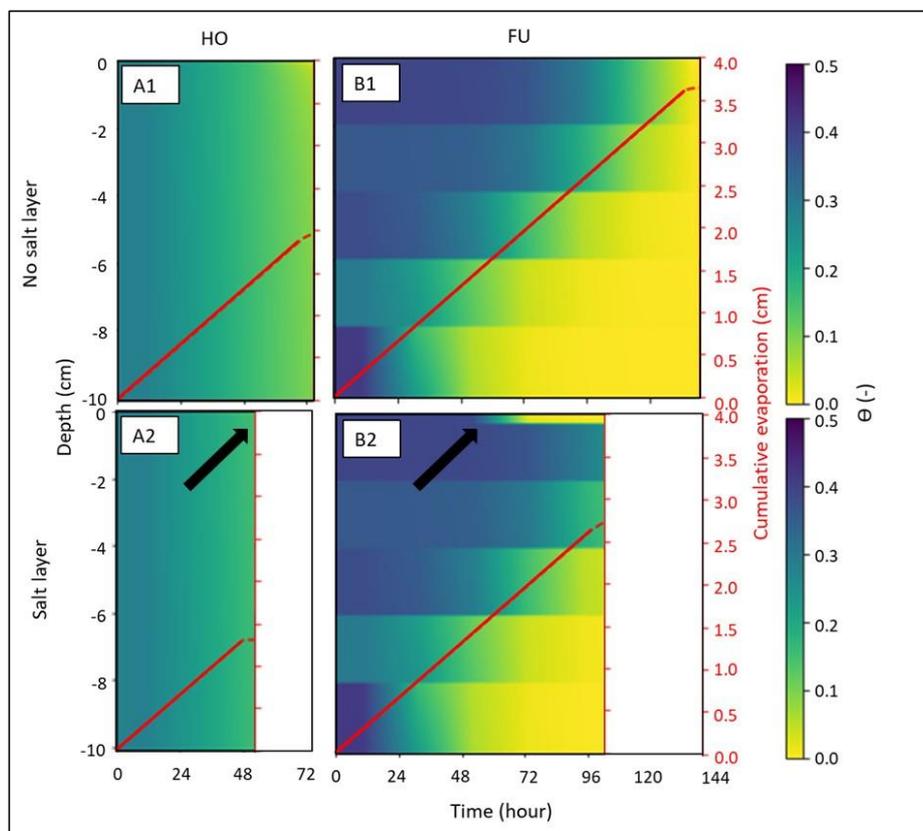
Figure 5: HYDRUS-1D simulations for temporal changes in water content (heat map) and
485   **cumulative evaporation (red curves). The continuous line corresponds to S1 evaporation,**
and dashed line, to the transition into S2 evaporation. The black arrows indicate the time of
the addition of the salt layer to the profile. (A) and (B) indicate on HO and FU setups,
respectively. (1) and (2) indicate the conditions of non-saline, and saline setups,
respectively.

490   While the numerical simulations strengthen the conceptual model and research hypotheses,

validation of the model and the physical processes presented by the conceptual model is

essential due to the numerical model limitations. These limitations include the lack of precise

and physically based information about the soil hydraulic properties in general and the salt

layer in particular. Moreover, as detailed above, the HYDRUS-1D model is reliable as long as

495   the hydraulic conditions permit to solve the Richards equation, which is not the case when the

system moves into S2 evaporation.   Therefore, the following column experiments were

conducted.

4.4. Evaporation and salt precipitation in layered porous media

As aforementioned, the column experiments were filled with glass beads as detailed in **Table**

500   **1**, and in a reverse order to mimic loose, e.g., tilled soil. The evaporation process during the

column experiments of the three glass beads configurations saturated with the saline solution

are represented by a set of pictures in **Figure 6**. It is possible to follow the movement of the

drying front for the neutral homogeneous configuration (HO), and the compacted (FU)

structures, which coincides with the numerical model results. Water flow and drying processes

505   are also observed for the tilled (CU) setup.

For the HO structure, the evaporation front receded from top to bottom, as typically seen in

evaporation of porous media, and a notable efflorescence salt crust was observed (**Figure 6A**).

Salt precipitation started after ~54 hours of evaporation.

For the FU structure, the soil surface remained moist for the entire duration of the

510   experiment, while the drying front progressed upward, from bottom to top (**Figure 6B**). The

unique drying pattern of the FU structure, which mimics compacted soil, is a result of the

hydraulic properties of the top layer that had the highest capillary suction along the soil

profile. This structure results in a continuous upward flow of the solution from the coarser

layers at the bottom that have a lower capillary suction. A similar behavior was reported by

515 Assouline and Narkis (2019) for DI water, where a detailed explanation of the impact of

layered structure on evaporation is given. For the FU setup, under saline conditions,

evaporation resulted in salt precipitation, at the soil surface, after ~54 hours of evaporation,

like in the HO case (**Figure 6B**).

For the CU structure, air penetration into the coarse upper layer was observed after 14 hours

520 of evaporation and a slow recession of the evaporation front downward was observed over

time (**Figure 6C**). For the CU case, no notable salt precipitation on the surface was observed.

Measurements and recording of changes in columns masses during the experiment enabled

to compute average cumulative evaporation, of the different setups, as presented in **Figure 7.**

Maximal values of standard deviation, for each setup, are detailed in **Table 2**. For the HO, the

525 duration of S1 with DI water was about 46 hours, with a cumulative evaporation of ~14 mm.

Total evaporation after 300 hours for the HO, DI water, was 23 mm. The relatively long S1

duration and high cumulative evaporation for HO, resulted in the formation of a notable

efflorescence salt crust (**Figure 6a**), with a thickness of about 3.5 mm as estimated from the

images. The saline conditions reduced the duration of S1 by more than 70%, and cumulative

530 evaporation at the transition from S1 to S2 was lowered by more than 50%, compared to

evaporation from initially DI saturated columns.

In agreement with the observed drying pattern (**Figure 6b**), it was shown that FU S1 was the

longest compared to all other setups (**Figure 7**). S1 duration for the FU structure was of 66 and

62 hours for the DI and saline conditions, respectively. Cumulative evaporation was also high

535 for the FU setup, with 11 and ~18 mm at the end of S1, for the saline solution and DI

conditions, respectively, and total cumulative evaporation after 300 hours, of 26 mm for the

saline solution, and 28 mm for the DI water. In comparison to the HO with DI water, the

cumulative evaporation of the FU, after 300 hours, was 13% higher (**Figure 7**). The long

duration of S1 for the FU, the persistence of the evaporation front at the surface of the

540   column, and the corresponding high cumulative evaporation (**Figure 7**), led to the

precipitation of a notable efflorescent salt crust (**Figure 6B**) with a thickness of about 6 mm as

estimated from the images.

While saline conditions for the HO setup led to reduction of more than 50% in total

evaporation and major changes in duration and cumulative evaporation of S1, for the FU

545   setup, the impact of salinity was much less prominent. For the FU, the salinity reduced

cumulative evaporation and the duration of S1 by less than 10%, and cumulative evaporation

at the transition from S1 to S2 was reduced by less than 40% (**Figure 7**).

Unlike for the HO setup, the evaporation from the CU column showed a transition from S1 to

S2 after ~19 hours of evaporation, and a cumulative evaporation of ~3.5 mm and ~4 mm

550   (**Figure 7**), for the saline solution and DI water, respectively. These results and the relatively

quick transition into S2, coincide with the receding of the evaporation front downward as seen

in **Figure 6c**. During S2, evaporation was minimal, due to the low rate of vapor diffusion

through the dry coarse porous medium at the surface, and total cumulative evaporation after

300 hours was 10 mm, for both saline and DI conditions, which is less than half the cumulative

555   evaporation of the HO setup and ~61% lower than the FU. As aforementioned, for the CU

saline conditions, no salt crust was observed because of the low cumulative evaporation, and

the receding evaporation front, that detained the processes of salinity buildup at the soil

surface. The absence of the salt crust at the surface of the CU column explains the observed

negligible difference in evaporation between the saline and DI water setups (**Figure 7**).

560
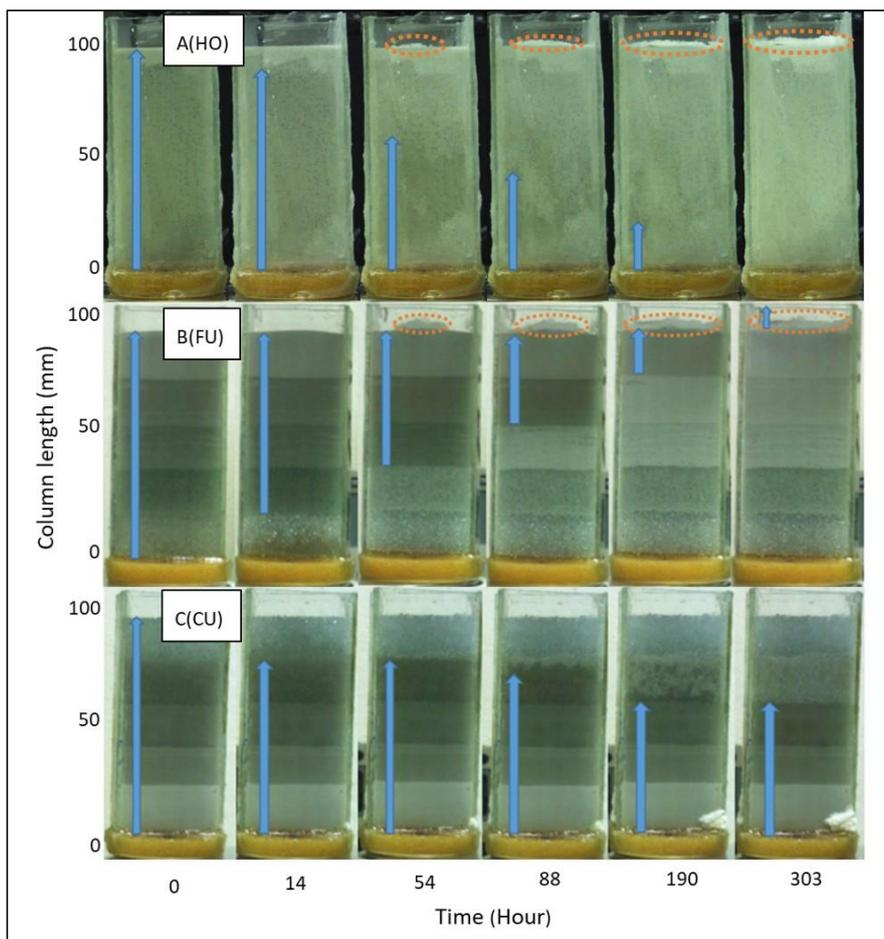
Figure 6: Evaporation and salt precipitation patterns for: (A) CU - with the coarse glass beads at the upper levels; (B) FU - with the fine glass beads at the upper levels; and (C) HO – homogeneous domain with the mixed glass beads. Numbers at the bottom indicate time length of evaporation. Top and bottom of the blue arrows indicate the upper and lower boundaries of the saturated zones, respectively. The orange circle marks locations of salt precipitation.

565
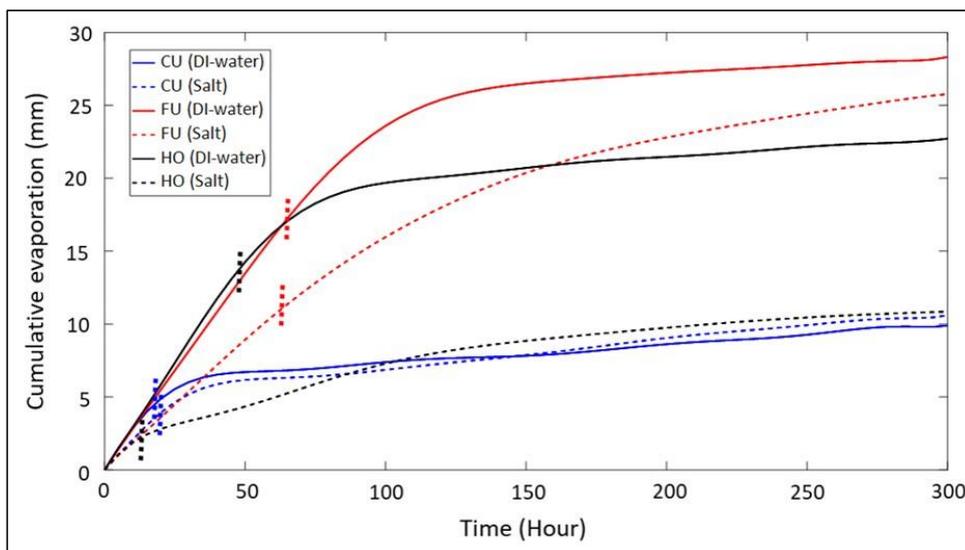
570

Figure 7: Cumulative evaporation for the coarse up (CU), fine up (FU), and the mixed (HO) structures, for conditions of DI water (solid lines) and saline solution (dashed lines). Vertical dotted lines indicate the transition from S1 to S2.

Table 2: Maximal values of standard deviation for cumulative evaporation measurements.

575

	DI - Water	Saline solution
HO	5.833	3.312
FU	5.928	4.957
CU	1.297	0.676

4.5. Differences in salinity impact on evaporation

As shown above, the three different setups: HO, FU, and CU, responded differently for the saline conditions, with the greatest impact observed for the HO, followed by the FU, and the

580   CU that presented minimal changes. **Figure 8** presents the relative change in cumulative evaporation for the different setups, over time. After ~5 hours of evaporation, all setups presented a reduction of about 30% in cumulative evaporation compared to the DI conditions. This reduction in evaporation may be a result of increased pore water NaCl concentration near the evaporation front at the surface of the columns, which results in reduction of the solution

585   osmotic potential and vapor pressure. The 30% reduction coincides with the fact that vapor pressure of a saturated NaCl solution, at 25 °C is equal to 2.401 kPa, which is ~25% lower than the vapor pressure of pure water that is equal to 3.169 kPa (Lide, 2007). However, more

interestingly, after these first five hours, the relative impact of salinity on evaporation started to vary significantly, depending on the soil structural configurations.

590   The HO setup introduced a reduction in evaporation that was much greater than 25%, at the order of 60%, throughout most of the evaporation process, with a maximal reduction of ~70% after about 50 hours. Total reduction in cumulative evaporation at the end of the experiment was around 50% (**Figure 8**). For the FU setup, the reduction in cumulative evaporation was maintained at 30-35% for about 100 hours, which is close to the S1 duration of the DI setup

595   (~70 hours). After ~100 hours, the difference between the saline and DI setups for FU was gradually moderated, along S2, and by the end of the experiment, total cumulative evaporation of the saline FU setup was only 10% lower compared to the DI state (**Figure 8**). For the CU setup, after the initial reduction of ~30% at the first five hours of evaporation, the difference between the saline and DI conditions decreased, to very low values, and after 150

600   hours of evaporation, no differences were observed (**Figure 8**).

For both HO and FU setups, the greatest difference in evaporation between the DI and saline conditions was observed during the time where the DI columns were at S1 and the saline solution configurations moved into S2. The large difference between the DI and saline condition for the HO during this time, at the order of 70%, indicates that the reduction of the

605   solution vapor pressure is not the only mechanism that reduces evaporation. For the non-saline condition the S1-S2 transition occurred after ~50 hours, for the HO setup. However, for the saline condition, S2 started after ~10 hours of evaporation only, with a minor cumulative evaporation at the order of 2mm.

From the HO-DI setup it is understood that at that time, the saline domain is moist enough to

610   supply water to the upper atmosphere-domain interface and that S1 should be sustained. Therefore, it is concluded that the transition into S2 after ~10 hours, is likely a result of salt precipitation and the development of the efflorescent salt crust on top of the HO domain. The

precipitated salt crust acts as a mulching layer that results in hydraulic discontinuity between the saturated domain and the atmosphere and vapor flow through the salt crust dictates the

615   evaporation rate. This is in agreement with observations from previous studies (Gran et al., 2011; Nachshon and Weisbrod, 2015), and the numerical simulation.

For the FU setup, the fact that the differences in duration of S1 between the DI and saline conditions were minor (**Figure 7**), and the reduction in cumulative evaporation during S1 is at the order of 30-35%, suggests that the main mechanism that reduced evaporation was the

620   reduction of the solution vapor pressure. The negligible impact of precipitated salt crust, for the FU setup, suggests that in this case the crust was hydraulically connected to the underlying media and that liquid water was flowing towards the surface of the salt crust, where the evaporation front was located. This hydraulic continuity suggests that the unique structure of the FU state, that mimics compacted soils, enables water from the lower layers of the drying

625   profile to flow upward into and through the salt crust. It is suggested here that the hydraulic continuity between the precipitated salt crust and the underlying domain was possible for the FU and not for HO, due to the unique FU structure that keeps the upper layer of the domain wet.

For the CU setup, it is believed that during S1, the increase of the NaCl solution concentration

630   at the evaporation front led to the observed reduction in evaporation at the order of 30%. This is in agreement with the vapor pressure reduction of a saturated NaCl solution. However, during S2 the differences between the DI and saline conditions decreased as vapor diffusivity, through the porous domain became the factor controlling evaporation, for both cases.

The differences in the impact of salinity on evaporation between the HO and FU setups

635   (**Figures 7-8**), together with the differences in patterns of drying (**Figure 6**), support the research hypothesis that even though more salt accumulation on the surface is expected in compacted conditions, its impact on evaporation is expected to be moderate compared to

neutral conditions, since the hydraulic connection to the surface persists longer and includes

the salt crust. We suggest that, in the case of a homogeneous soil, the receding evaporation

640 front breaks the hydraulic continuity to the salt crust. The water vapor diffusion process is

therefore slowed down by the addition, on top of the soil surface, of the dry salt crust that

acts as a mulching layer. For the FU setup, the high water content which is maintained at the

soil surface throughout the evaporation process, sustains the hydraulic continuity from the

saturated domain through the salt crust, towards its upper surface.

645
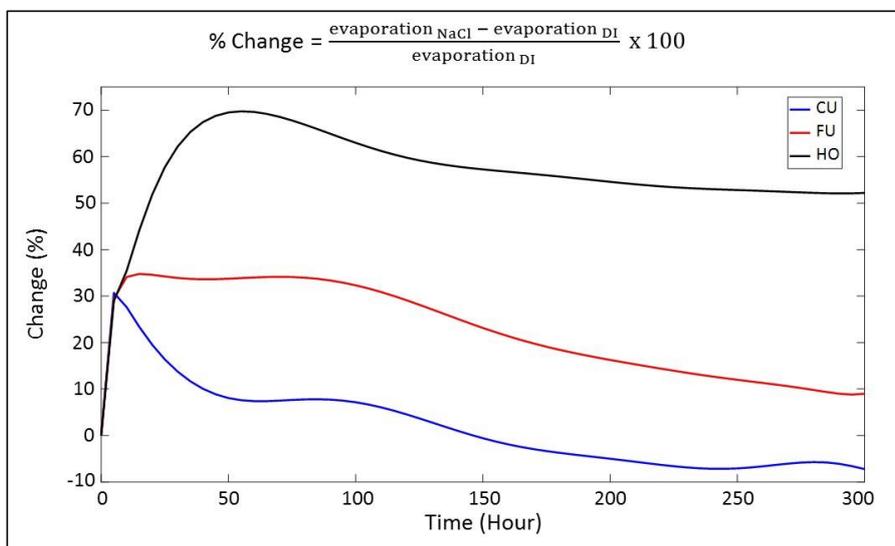
Figure 8: Relative difference in cumulative evaporation between saline and non-saline soil
650 **water solution over time, for the loose (CU), homogeneous (HO), and compacted (FU)**
setups.

5. Summary and Conclusions

This study investigates the effect of compaction on sand physical properties at the micro and

655 macro scales, and its impact on evaporation combined with salt precipitation processes.

Microscale properties such as the geometrical pore parameters were studied using X-ray

computed micro-tomography (μCT) techniques by scanning sand samples before and after

compaction. Compaction resulted in breakage of sand grains, reduced grain sizes, and pore

average opening, mainly close to the source of compression. The spatial distribution of grain

660 number, for the top levels of the compacted domain, has a higher proportion of areas with

more grain numbers than the non-compacted and the lower levels of the compacted samples.

These results illustrated the non-uniform spatial distribution of the physical changes that the

soil undergoes through compaction. The impact of compaction decreases with depth, away

from the source of compression.

665 Macro-scale soil compaction changes were evaluated by analyzing images that captured the

movement of colored sand grains and measuring their translocation before and after

compaction. The highest translocation was at the upper levels of the soil profile, and with

depth, translocation decreased. The distances between adjacent selected grains, before and

following compaction, indicated that compaction is not uniform along the sand profile, with

670 certain levels compacted more than others, strengthening the assumption of the

heterogeneous nature of soil compaction and the shear band effect.

Since compaction affects the particle arrangement along the profile in a non-uniform manner,

with maximal compaction at the relatively high layers of the soil profile, the impact of

compaction on combined evaporation and salt precipitation was observed using layered

675 columns packed with glass beads with increasing size with depth (FU). A reference setup

consisted of a homogeneous column packed with mixed glass beads sizes (HO). In opposition

to the compacted setup, a layered column where the glass beads sizes decreased with depth

represented a tilled soil profile (CU). The cumulative evaporation measurements and the

visual observations pointed to the significant impact of the different configurations on

680 combined processes of evaporation and salt precipitation.

For the HO structure, the evaporation front recedes from top to bottom. The relatively long

S1 duration and high cumulative evaporation for the HO setup resulted in a notable

precipitation of an efflorescence salt crust. The precipitated salt layer resulted in a sharp

decrease in evaporation rate since hydraulic continuity to the surface is ceased, and the slow

685   process of vapor diffusion through the salt layer controls evaporation.

For the FU, the drying front propagated from bottom to top. S1 duration of the FU was long for the saline and DI water, and the cumulative evaporation was high, which led to prominent efflorescent salt crust precipitation at the surface. However, in contrast to the HO, even though a notable salt layer was observed, its impact on evaporation at the FU structure was

690   moderated compared to its impact for the HO setup. This is attributed to the stronger capillary suction of the upper layers, at the FU structure, which pumps water from the underlying levels upwards, maintaining high saturation at the soil surface, which supports liquid water continuity from the soil to the evaporation front, at the salt crust upper surface.

For CU setup, a moderate recession of the evaporation front downward occurred over time

695   like in the HO configuration, and loss of hydraulic continuity to the surface was achieved relatively early. Thus, the cumulative evaporation was low, salt precipitation was minor and therefore negligible differences in evaporation between saline and non-saline conditions were observed.

This work sheds new light on the impact that soil compaction, which is a common feature in

700   arable lands, has on bare soil evaporation processes, for saline and non-saline conditions. Future studies should examine the findings of this study, under field conditions and to determine whether the observed phenomena occur in the field, where the 3-D expression of natural compaction will not necessarily create a layered soil profile. However, the insights gained from this study indicate that one may consider the use of different agricultural

705   practices to control the degree of soil compaction, to the benefit of the water regime in the root zone.

6. References

Akker, J.J.H., Canarache, A., 2001. Two European concerted actions on subsoil compaction.

710   Landnutzung und Landentwicklung 42, 15–22.

Alaoui, A., J. Lipiec, and H.H. Gerke. 2011. A review of the changes in the soil pore system

due to soil deformation: A hydrodynamic perspective. Soil Tillage Res. 115–116: 1–15.

doi: 10.1016/j.still.2011.06.002.

Alaoui, A., M. Rogger, S. Peth, and G. Blöschl. 2018. Does soil compaction increase floods? A

715   review. J. Hydrol. 557(January): 631–642. doi: 10.1016/j.jhydrol.2017.12.052.

de Almeida, W.S., E. Panachuki, P.T.S. de Oliveira, R. da Silva Menezes, T.A. Sobrinho, et al.

2018. Effect of soil tillage and vegetal cover on soil water infiltration. Soil Tillage Res.

175(June 2017): 130–138. doi: 10.1016/j.still.2017.07.009.

Assouline, S. 2004. Rainfall-Induced Soil Surface Sealing: A Critical Review of Observations,

720   Conceptual Models, and Solutions. Vadose Zo. J. 3(2): 570–591. doi:

10.2136/vzj2004.0570.

Assouline, S. 2006a. Modeling the Relationship between Soil Bulk Density and the Hydraulic

Conductivity Function. Vadose Zo. J. 5(2): 697–705. doi: 10.2136/vzj2005.0084.

Assouline, S. 2006b. Modeling the Relationship between Soil Bulk Density and the Water

725   Retention Curve. Vadose Zo. J. 5(2): 554–563. doi: 10.2136/vzj2005.0083.

Assouline, S., and T. Kamai. 2019. Liquid and Vapor Water in Vadose Zone Profiles Above

Deep Aquifers in Hyper-Arid Environments. Water Resour. Res. 55(5): 3619–3631. doi:

10.1029/2018WR024435.

Assouline, S., and K. Narkis. 2019. Evaporation From Multilayered Heterogeneous Bare Soil

730   Profiles. Water Resour. Res. 55(7): 5770–5783. doi: 10.1029/2018wr024560.

Assouline, S., K. Narkis, R. Gherabli, P. Lefort, and M. Prat. 2014. Analysis of the impact of

surface layer properties on evaporation from porous systems using column

experiments and modified definition of characteristic length. doi: 10.1111/j.1752-

1688.1969.tb04897.x.

735   Assouline, S., and D. Or. 2006. Anisotropy factor of saturated and unsaturated soils. Water
Resour. Res. 42(12): 1–11. doi: 10.1029/2006WR005001.

Assouline, S., J.S. Selker, and J.Y. Parlange. 2007. A simple accurate method to predict time
of ponding under variable intensity rainfall. Water Resour. Res. 43(3): 1–10. doi:
10.1029/2006WR005138.

740   Augeard, B., S. Assouline, A. Fonty, C. Kao, and M. Vauclin. 2007. Estimating hydraulic
properties of rainfall-induced soil surface seals from infiltration experiments and X-ray
bulk density measurements. J. Hydrol. 341(1–2): 12–26. doi:
10.1016/j.jhydrol.2007.04.018.

Barik, K., E.L. Aksakal, K.R. Islam, S. Sari, and I. Angin. 2014. Spatial variability in soil

745   compaction properties associated with field traffic operations. Catena 120: 122–133.
doi: 10.1016/j.catena.2014.04.013.

Benson, C.H., I. Chiang, T. Chalermyanont, and A. Sawangsuriya. 2014. Estimating van
Genuchten Parameters α and n for Clean Sands from Particle Size Distribution Data.
From Soil Behavior Fundamentals to Innovations in Geotechnical Engineering. doi:

750   10.1061/9780784413265.033.

Berezniak, A., A. Ben-Gal, Y. Mishael, and U. Nachshon. 2018. Manipulation of Soil Texture to
Remove Salts from a Drip-Irrigated Root Zone. Vadose Zo. J. 17(1): 170019. doi:
10.2136/vzj2017.01.0019.

Bergstad, M., D. Or, P.J. Withers, and N. Shokri. 2017. The influence of NaCl concentration on

755   salt precipitation in heterogeneous porous media. Water Resour. Res. 53: 1702–1713.
doi: 10.1002/2016WR020060.

Bergstad, M., D. Or, P.J. Withers, and N. Shokri. 2018. Evaporation Dynamics and NaCl
Precipitation on Capillarity-Coupled Heterogeneous Porous Surfaces. Water Resour.
Res. 54(6): 3876–3885. doi: 10.1029/2018WR022614.

760   Bresson, L.M., C.J. Moran, and S. Assouline. 2004. Use of Bulk Density Profiles from X-

Radiography to Examine Structural Crust Models. Soil Sci. Soc. Am. J. 68(4): 1169–1176.

doi: 10.2136/sssaj2004.1169.

Brutsaert, W. 2005. Hydrology: An Introduction. Cambridge Univ. Press, New York.

Campbell, D.J. 1994. Determination and Use of Soil Bulk Density in Relation to Soil

765   Compaction. Dev. Agric. Eng. 11(C): 113–139. doi: 10.1016/B978-0-444-88286-8.50014-

3.

Carman, P.C. 1937. Fluid flow through a granular bed. Transactions of the Institution of

Chemical Engineers. : 15, 150–156.

Dejong-Hughes, J., J. Moncrief, W.. Voorhees, and J.. Swan. 2001. soil compaction causes

770   effects and control. : 1–16.

Gran, M., J. Carrera, S. Olivella, and M.W. Saaltink. 2011. Modeling evaporation processes in

a saline soil from saturation to oven dry conditions. Hydrol. Earth Syst. Sci. 15(7): 2077–

2089. doi: 10.5194/hess-15-2077-2011.

Hamza, M.A., and W.K. Anderson. 2005. Soil compaction in cropping systems: A review of

775   the nature, causes and possible solutions. Soil Tillage Res. 82(2): 121–145. doi:

10.1016/j.still.2004.08.009.

Hendrickx, J.M.., and M. Flury. 2001. Uniform and preferential flow mechanisms in the

vadose zone. Concept. Model. Flow Transp. Fract. Vadose Zo. Natl. Acad. Press.

Washington, D.C,: 149–187.

780   Hernanz, J.L., H. Peixoto, C. Cerisola, and V. Sánchez-Girón. 2000. An empirical model to

predict soil bulk density profiles in field conditions using penetration resistance,

moisture content and soil depth. J. Terramechanics 37(4): 167–184. doi:

10.1016/S0022-4898(99)00020-8.

Hillel, D. 1980. Introduction to Soil Physics. Academic Press, London.

785   Hopmans, J.W., A.S. Qureshi, I. Kisekka, R. Munns, S.R. Grattan, et al. 2021. Critical

knowledge gaps and research priorities in global soil salinity.

Horn, R., H. Domial, A. Slowihka-Jurkiewiczb, and C. Van Ouwerkerkct. 1995. Soil compaction

processes and their effects on the structure of arable soils and the environment.

Elsevier Sci. B.V.Soil Tillage Res. 35(35): 23–36. doi: 10.1016/0167-1987(95)00479-C.

790   Horton, R., M.. Ankeny, and R.. Allmaras. 1994. Effects of Compaction on Soil Hydraulic

Properties. Soil Compaction in Crop Production. p. 141–165

Kamai, T., and S. Assouline. 2018. Evaporation From Deep Aquifers in Arid Regions:

Analytical Model for Combined Liquid and Vapor Water Fluxes. Water Resour. Res.

54(7): 4805–4822. doi: 10.1029/2018WR023030.

795   Kasenow, M. 2002. Determination of hydraulic conductivity from grain size analysis. Water

Resources Publication, New York.

Keller, T., M. Lamandé, S. Peth, M. Berli, J.Y. Delenne, et al. 2013. An interdisciplinary

approach towards improved understanding of soil deformation during compaction. Soil

Tillage Res. 128: 61–80. doi: 10.1016/j.still.2012.10.004.

800   Keller, T., M. Sandin, T. Colombi, R. Horn, and D. Or. 2019. Historical increase in agricultural

machinery weights enhanced soil stress levels and adversely affected soil functioning.

Soil Tillage Res. 194(June). doi: 10.1016/j.still.2019.104293.

Kozeny, J. 1927. Uber kapillare Leitung des Wassers im Boden. Sitzungsber. Akad. Wiss. :

136, 271–306.

805   Lehmann, P., S. Assouline, and D. Or. 2008. Characteristic lengths affecting evaporative

drying of porous media. Phys. Rev. E - Stat. Nonlinear, Soft Matter Phys. 77(5): 1–16.

doi: 10.1103/PhysRevE.77.056309.

Lehmann, P., and D. Or. 2009. Evaporation and capillary coupling across vertical textural

contrasts in porous media. Phys. Rev. E - Stat. Nonlinear, Soft Matter Phys. 80(4): 1–13.

810   doi: 10.1103/PhysRevE.80.046318.

Lide, R.D. (ed.). 2007. CRC Handbook of Chemistry and Physics. CRC, Boca Raton.

Lipiec, J., and W. Stępniewski. 1995. Effects of soil compaction and tillage systems on uptake and losses of nutrients. Soil Tillage Res. 35(1–2): 37–52. doi: 10.1016/0167-1987(95)00474-7.

815   Mossadeghi-Björklund, M., J. Arvidsson, T. Keller, J. Koestel, M. Lamandé, et al. 2016. Effects of subsoil compaction on hydraulic properties and preferential flow in a Swedish clay soil. Soil Tillage Res. 156: 91–98. doi: 10.1016/j.still.2015.09.013.

Mossadeghi-Björklund, M., N. Jarvis, M. Larsbo, J. Forkman, and T. Keller. 2018. Effects of compaction on soil hydraulic properties, penetration resistance and water flow

820   patterns at the soil profile scale (M. Goss, editor). Soil Use Manag. 35(3): 367–377. doi: 10.1111/sum.12481.

Nachshon, U. 2016. Seepage weathering impacts on erosivity of arid stream banks: A new conceptual model. Geomorphology 261: 212–221. doi: 10.1016/j.geomorph.2016.03.011.

825   Nachshon, U. 2018. Cropland soil salinization and associated hydrology: Trends, processes and examples. Water (Switzerland) 10(8). doi: 10.3390/w10081030.

Nachshon, U., E. Shahraeeni, D. Or, M. Dragila, and N. Weisbrod. 2011a. Infrared thermography of evaporative fluxes and dynamics of salt deposition on heterogeneous porous surfaces. Water Resour. Res. 47(12): 1–16. doi: 10.1029/2011WR010776.

830   Nachshon, U., and N. Weisbrod. 2015. Beyond the Salt Crust: On Combined Evaporation and Subflorescent Salt Precipitation in Porous Media. Transp. Porous Media 110(2): 295–310. doi: 10.1007/s11242-015-0514-9.

Nachshon, U., N. Weisbrod, M.I. Dragila, and A. Grader. 2011b. Combined evaporation and salt precipitation in homogeneous and heterogeneous porous media. Water Resour.

835   Res. 47(3): 1–16. doi: 10.1029/2010WR009677.

Nassar, I.N., and R. Horton. 1997. Heat, Water, and Solute Transfer in Unsaturated Porous Media: I - Theory Development and Transport Coefficient Evaluation. Transp. Porous

Media 27(1): 17–38. doi: 10.1023/A:1006583918576.

Nassar, I.N., and R. Horton. 1999. Salinity and compaction effects on soil water evaporation

840   and water and solute distributions. Soil Sci. Soc. Am. J. 63(4): 752–758. doi:

10.2136/sssaj1999.634752x.

Naveed, M., P. Schjønning, T. Keller, L.W. de Jonge, P. Moldrup, et al. 2016. Quantifying

vertical stress transmission and compaction-induced soil structure using sensor mat

and X-ray computed tomography. Soil Tillage Res. 158(October 2017): 110–122. doi:

845   10.1016/j.still.2015.12.006.

Nawaz, M.F., G. Bourrié, and F. Trolard. 2013. Soil compaction impact and modelling. A

review. Agron. Sustain. Dev. 33(2): 291–309. doi: 10.1007/s13593-011-0071-8.

Or, D., P. Lehmann, E. Shahraeeni, and N. Shokri. 2013. Advances in Soil Evaporation Physics-

A Review. Vadose Zo. J. 12(4): vzj2012.0163. doi: 10.2136/vzj2012.0163.

850   Otsu, N. 1979. A Threshold Selection Method from Gray-Level Histograms. IEEE Trans. Syst.

Man. Cybern. 9(1): 62–66. doi: 10.1109/TSMC.1979.4310076.

Pagliai, M., A. Marsili, P. Servadio, N. Vignozzi, and S. Pellegrini. 2003. Changes in some

physical properties of a clay soil in Central Italy following the passage of rubber tracked

and wheeled tractors of medium power. Soil Tillage Res. 73(1–2): 119–129. doi:

855   10.1016/S0167-1987(03)00105-3.

Piotrowski, J., J.A. Huisman, U. Nachshon, A. Pohlmeier, and H. Vereecken. 2020. Gas

permeability of salt crusts formed by evaporation from Porous media. Geosci. 10(11):

1–19. doi: 10.3390/geosciences10110423.

Prat, M. 2002. Recent advances in pore-scale models for drying of porous media. Chem. Eng.

860   J. 86(1–2): 153–164. doi: 10.1016/S1385-8947(01)00283-2.

Rad, M.N., and N. Shokri. 2012. Nonlinear effects of salt concentrations on evaporation from

porous media. 39(January): 1–5. doi: 10.1029/2011GL050763.

Rasmussen, K.J. 1999. Impact of ploughless soil tillage on yield and soil quality: A

Scandinavian review. Soil Tillage Res. 53(1): 3–14. doi: 10.1016/S0167-1987(99)00072-

865   0.

Reicosky, D.C., W.B. Voorhees, and J.K. Radke. 1981. Unsaturated Water Flow Through a

Simulated Wheel Track1. Soil Sci. Soc. Am. J. 45(1): 3. doi:

10.2136/sssaj1981.03615995004500010001x.

Schlüter, S., and H.J. Vogel. 2016. Analysis of soil structure turnover with garnet particles and

870   X-Ray microtomography. PLoS One 11(7): 1–17. doi: 10.1371/journal.pone.0159948.

Shah, A.N., M. Tanveer, B. Shahzad, G. Yang, S. Fahad, et al. 2017. Soil compaction effects on

soil health and cropproductivity: an overview. Environ. Sci. Pollut. Res. 24(11): 10056–

10067. doi: 10.1007/s11356-017-8421-y.

Shokri-kuehni, S.M.S., M. Norouzi, C. Webb, N. Shokri, C. Zeiss, et al. 2017. Advances in

875   Water Resources Impact of type of salt and ambient conditions on saline water

evaporation from porous media. 105: 154–161. doi: 10.1016/j.advwatres.2017.05.004.

Shokri-Kuehni, S.M.S., T. Vetter, C. Webb, and N. Shokri. 2017. New insights into saline water

evaporation from porous media: Complex interaction between evaporation rates,

precipitation, and surface temperature. Geophys. Res. Lett. 44(11): 5504–5510. doi:

880   10.1002/2017GL073337.

Shokri, N., P. Lehmann, and D. Or. 2010. Evaporation from layered porous media. J. Geophys.

Res. Solid Earth 115(6): 1–12. doi: 10.1029/2009JB006743.

Sillon, J.F., G. Richard, and I. Cousin. 2003. Tillage and traffic effects on soil hydraulic

properties and evaporation. Geoderma 116(1–2): 29–46. doi: 10.1016/S0016-

885   7061(03)00092-2.

Šimůnek, J., A. M. Šejna, H. Saito, M. Sakai, and M.T. Van Genuchten. 2013. The HYDRUS-1D

software package for simulating the movement of water, heat, and multiple solutes in

variably saturated media, version 4.17. HYDRUS Softw. Ser. 3D (June): 343.

Soane, B.D., and C. van Ouwerkerk. 1995. Implications of soil compaction in crop production

890   for the quality of the environment. Soil Tillage Res. 35(1–2): 5–22. doi: 10.1016/0167-

1987(95)00475-8.

El Titi, A. 2003. Soil Tillage in Agroecosystems. CRC Press, Boca Raton/London/New

York/Washington D.C.

Wang, J.-P., N. Hu, B. Françoise, and P. Lambert. 2017. Estimating water retention curves and

895   strength properties of unsaturated sandy soils from basic soil gradation parameters.

Water Resour. Res. 53: 6069–6088. doi: 10.1002/2017WR020411.Received.

Weisbrod, N., U. Nachshon, M. Dragila, and A. Grader. 2013. Micro-CT Analysis to Explore

Salt Precipitation Impact on Porous Media Permeability. : 231–241. doi:

doi:10.1007/978-94-007-7534-3_20.

900   Yakirevich, A., N. Weisbrod, M. Kuznetsov, C.A. Rivera Villarreyes, I. Benavent, et al. 2013.

Modeling the impact of solute recycling on groundwater salinization under irrigated

lands: A study of the Alto Piura aquifer, Peru. J. Hydrol. 482: 25–39. doi:

10.1016/j.jhydrol.2012.12.029.

905